Scarfed Nozzles for Thrust-Vector Adjustment

Jay S. Lilley* and Jerrold H. Arszman†
U.S. Army Missile Command, Redstone Arsenal, Alabama 35898

This paper presents the results of an investigation into the utilization of scarfed nozzles for thrust-vector adjustment. The investigation was conducted to determine the feasibility of utilizing scarfed nozzles on tactical missiles employing multiple strap-on solid rocket boosters. This approach offers an effective and low-cost method for aligning the thrust vector with the missile center of gravity. The use of such nozzles provides a means of minimizing the impact of booster-to-booster performance variation on missile angular velocity while having a minimal impact on individual booster performance. A previously developed scarfed nozzle performance-prediction computer code served as the primary theoretical analysis tool. This code was utilized to conduct an extensive parametric study that characterized the influence of scarfed nozzle geometry and nozzle operating pressure on the direction and magnitude of the thrust vector. The influence of scarfed nozzle geometry on the thrust vector was also experimentally investigated by statically firing specially designed solid rocket motors that employed scarfed nozzles. The data from the experimental motor firing were compared to performance predictions generated by the theoretical model. Design implications and concept limitations are addressed.

Nomenclature

A = downstream throat-attachment point
A_t = throat area
C_F = thrust coefficient
C_M = moment coefficient
E = scarfed extension starting point
F = thrust, scarfed extension ending point
M = side-force action point, moment
$\dot{m}$ = mass flow rate
P = pressure
T = throat
u = nozzle axial velocity component
X = motor axial coordinate
x = nozzle axial coordinate
Y = motor radial coordinate
y = nozzle radial coordinate
α = basic nozzle half-angle
β = scarf angle
γ = specific heat ratio
ϵ = expansion ratio
η = efficiency
θ_T = thrust angle
ρ = throat-curvature radius
ψ = scarf cut integration half-angle

Subscripts

a = ambient
bn = basic nozzle
e = scarfed extension starting point
exp = experimental
f = scarfed extension ending point
IVL = initial value line
m = side-force action point
t = stagnation, throat
td = throat downstream
th = theoretical
tu = throat upstream
vac = vacuum
X = motor axial coordinate, motor axial thrust
x = nozzle axial coordinate
Y = motor radial coordinate, motor radial thrust
y = nozzle radial coordinate
θ = thrust angle

Introduction

FOR certain tactical missile designs, it is desirable to employ several strap-on solid rocket boosters attached circumferentially around a centerbody. However, this propulsion system concept creates significant problems for the missile designer. The performance of each individual booster will be subject to the motor-to-motor variability in thrust level and burn time that is normally associated with solid rocket motors. During booster operations, the thrust-level differences between the individual rocket motors will result in a moment about the missile center of gravity. The differences in burn time among the various motors will also generate significant moments as each motor will cease operation at different times. Any moments generated by the propulsion system will have an adverse impact on the design of the guidance and control system for the missile. Consequently, it is desirable to eliminate these moments.

The obvious method to eliminate the moments generated by the propulsion system is to adjust the thrust vector for each individual booster so that it passes through the missile center of gravity. An active thrust-vector control system is not a viable consideration due to the cost and weight restrictions imposed on most tactical missile systems. Consequently, a passive means of thrust-vector adjustment is required. Conventional approaches to achieve this objective would be to cant the nozzle of each booster or to use a tapered motor case and cant the entire motor. Both of these approaches complicate the design of the booster, increase the propulsion system cost, and incur a performance loss as the axial thrust of the rocket motor acts at an angle to the missile centerline. It is evident that an alternate approach that has minimal impact on the booster cost and performance is required to adjust the thrust vector.

An attractive alternative is to employ a scarfed nozzle on each booster. Each scarfed nozzle consists of a conventional axisymmetric conical nozzle with a truncated (scarfed) cylindrical extension. An illustration of a possible booster design is shown in Fig. 1. The axis of the nozzle is colinear with the booster axis and parallel to the missile axis so that no axial thrust loss exists and conventional booster design practices can

Received July 18, 1989; revision received Feb. 5, 1990.

*Aerospace Engineer, Propulsion Directorate. Member AIAA.
†Physicist, Propulsion Directorate.

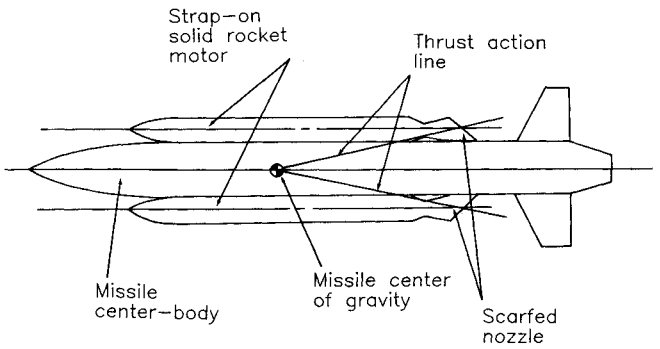

Fig. 1 Possible scarfed nozzle application.

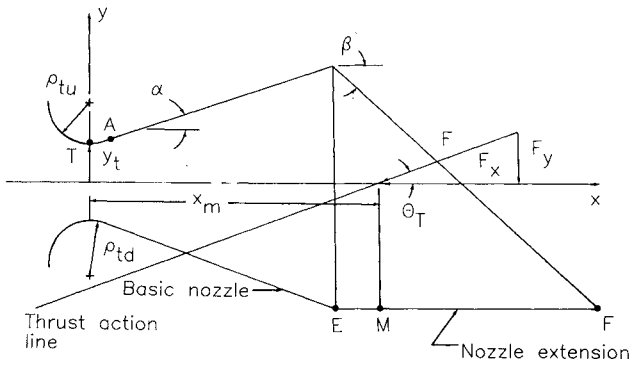

Fig. 2 Geometric model.

be employed. Control of the thrust-vector direction is achieved by the scarfed extension that generates a side force normal to the missile axis. By varying the unscarfed nozzle geometry and the length of the scarfed extension, the magnitude of the side force can be adjusted such that the resultant thrust vector passes through the center of the gravity of the missile.

The addition of the scarfed extension does not influence the motor axial thrust of the booster. Consequently, no performance penalty is incurred for generating the side force unlike the case of the canted nozzle or motor. However, the particular missile system design may require thermal protection to shield the centerbody from the impingement of gas. If required, the relative impact of this protection on system cost or weight should be insignificant for tactical boosters that have typically short burn times. Therefore, the use of a scarfed extension offers a method of adjusting the booster thrust vector that has minimal impact on propulsion system cost or performance.

An investigation was conducted to evaluate the use of scarfed nozzles for thrust-vector adjustment. A theoretical performance-prediction model for scarfed nozzles was developed based on a computer code that had been applied extensively in previous investigations of canted, scarfed nozzles.[1] Using this performance model, a parametric study was conducted to characterize the influence of scarfed nozzle geometry and motor operating conditions on thrust-vector adjustment. Static test firings of specially designed solid rocket motors that employed a variety of scarfed nozzle configurations were conducted to validate the theoretical model. Limitations on the application of scarfed nozzles for thrust-vector adjustment are discussed.

Analysis Model

The theoretical analysis model utilized in this investigation is a modification of a scarfed nozzle performance-analysis computer code developed by Hoffman.[2] This code was used extensively in previous scarfed nozzle performance studies[1] and has been experimentally validated with data from numerous solid rocket motor firings.[1,3] Descriptions of the geometric model, the flowfield model, and the performance model utilized in the computer code are as follows.

Geometric Model

A plane view of the scarfed nozzle geometric model is shown in Fig. 2. The basic nozzle consists of a double circular arc throat contour joined smoothly to a conical supersonic expansion contour. The nozzle extension consists of a truncated (scarfed) cylindrical section beginning at the end of the basic nozzle.

The throat geometry is completely specified by the throat radius y_t, the upstream and downstream throat curvature radii ρ_{tu} and ρ_{td}, respectively, and the cone angle α. The two circular arcs join smoothly at the throat point T. The downstream circular arc attaches smoothly to the conical expansion contour at point A. The basic nozzle contour is specified by the cone half-angle α and the expansion ratio ϵ. The expansion ratio is given by

$$\epsilon = (y_e/y_t)^2 \tag{1}$$

where y_e is the radius of the cone at the end of the basic nozzle (point E). The nozzle extension is a cylinder with radius y_e that is joined to the basic nozzle forming a discontinuity in the nozzle wall at point E. The cylindrical extension is truncated by a planar cut that passes through point E at an angle β and terminates at point F. For a given basic nozzle contour, the nozzle extension is completely specified by the scarf angle β.

In this analysis, the axis of the nozzle x is assumed to be colinear to the motor axis X and parallel to the missile axis. The scarfed exit plane of the nozzle is oriented through the missile axis (to prevent any roll moments) and faces aftward and outward in relation to the missile centerbody (see Fig. 1). The present orientation of the nozzle differs greatly from typical scarfed nozzle applications where the nozzle axis is canted such that the exit plane is flush with the missile skin.

Flowfield Model

An axisymmetric numerical method-of-characteristics analysis was utilized to determine the scarfed nozzle flowfield. This analysis was developed by Hoffman and is described in detail in Ref. 2. Different flowfield analyses were employed depending on nozzle region—for the throat region, a transonic analysis; in the basic nozzle up to the region of influence of the discontinuity (point E), an irrotational analysis; at the wall discontinuity, an oblique shock wave analysis; and down-

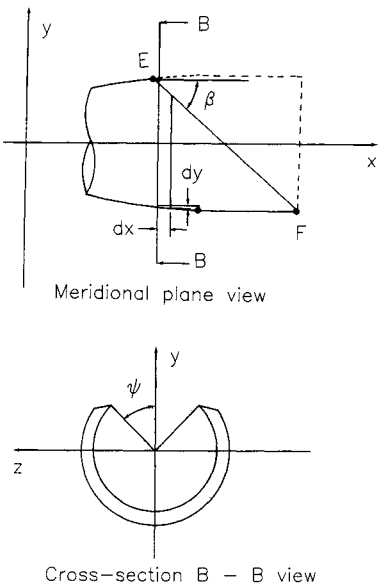

Fig. 3 Performance model.

stream of the shock wave, a rotational analysis. Extensive experimental investigations have shown this flowfield model to be a valid tool for the analysis of scarfed nozzles utilized in tactical solid propulsion systems.[1,3,4]

Performance Model

The nozzle wall pressure distribution predicted by the flowfield analysis is intergrated over the wall geometry to obtain the nozzle performance. The two factors of interest in characterizing the performance of the scarfed nozzle are motor axial thrust coefficient $C_{F,X}$ and thrust angle θ_T. Another geometric parameter of interest is the nozzle side-thrust action location x_m.

The approach used in determining nozzle performance is to calculate the performance under vacuum conditions and then correct for atmospheric pressure. The vacuum motor axial thrust coefficient $C_{F,X_{\text{vac}}}$ is given by

$$C_{F,X_{\text{vac}}} = C_{F,X_{\text{IVL}}} + C_{F,X_{bn_{\text{vac}}}} \tag{2}$$

where $C_{F,X_{\text{IVL}}}$ is the motor axial vacuum-thrust coefficient of the throat and $C_{F,X_{bn_{\text{vac}}}}$ is the motor axial vacuum-thrust coefficient of the basic nozzle conical expansion contour.

These thrust coefficients are given by

$$C_{F,X_{\text{IVL}_{\text{vac}}}} = [1/(A_t P_t)] \int_{\text{IVL}} (2\pi y\, P\,\mathrm{d}y + u\,\mathrm{d}\dot{m}) \tag{3}$$

$$C_{F,X_{bn_{\text{vac}}}} = 2\pi\,/A_t \int_{y_t}^{y_e} (P/P_t) y\,\mathrm{d}y \tag{4}$$

where

$$A_t = \pi y_t^2 \tag{5}$$

Note that the integration for the motor axial thrust coefficient is only over the unscarfed section of the nozzle since the cylindrical scarfed extension is parallel to the motor axis and thus produces no axial thrust. This effect is counter to most tactical scarfed nozzles that are usually canted to the motor centerline.

The motor side vacuum-thrust coefficient is given by

$$C_{F,Y_{\text{vac}}} = 2/A_t \int_{x_e}^{x_f} (P/P_t) y \sin\psi\ \mathrm{d}x \tag{6}$$

where x_e is the nozzle axial coordinate of point E, x_f is the nozzle axial coordinate of point F, and ψ is the half-angle of the scarf cut. The angle ψ and the integration procedure are shown in Fig. 3. Note that the integration for the side-thrust coefficient is only over the scarfed extension since the start of the scarf cut and the start of the cylindrical extension both occur at point E. Consequently, only the cylindrical extension generates side thrust. The nozzle side vacuum-moment coefficient $C_{M_{\text{vac}}}$ is given by

$$C_{M_{\text{vac}}} = 2/(A_t y_t) \int_{x_e}^{x_f} (P/P_t)\, xy \sin\psi\ \mathrm{d}x \tag{7}$$

where the vacuum nozzle axial location of the side force $x_{m_{\text{vac}}}$ is given by

$$x_{m_{\text{vac}}} = y_t C_{M_{\text{vac}}}/C_{F,Y_{\text{vac}}} \tag{8}$$

The contribution of the ambient pressure P_a to nozzle performance is given by

$$C_{F,X_a} = (P_a/P_t)\,\epsilon \tag{9}$$

$$C_{F,Y_a} = C_{F,X_a}/\tan\beta \tag{10}$$

$$x_{m_a} = y_e/\tan\beta + x_e \tag{11}$$

$$C_{M_a} = C_{F,Y_a} x_{m_a}/y_t \tag{12}$$

where the subscript a denotes the contribution of atmospheric pressure to the respective performance factors.

The performance of the nozzle is determined by subtracting the contribution of the atmospheric pressure from the vacuum-performance factors. The nozzle performance factors are given by

$$C_{F,X} = C_{F,X_{\text{vac}}} - C_{F,X_a} \tag{13}$$

$$C_{F,Y} = C_{F,Y_{\text{vac}}} - C_{F,Y_a} \tag{14}$$

$$C_M = C_{M_{\text{vac}}} - C_{M_a} \tag{15}$$

$$x_m = y_t C_M/C_{F,Y} \tag{16}$$

$$\theta_T = \tan^{-1}(C_{F,Y}/C_{F,X}) \tag{17}$$

It should be noted that the thrust coefficients integrated over the nozzle coordinates x and y also apply to the motor coordinates X and Y since the nozzle axis is colinear to the motor axis. However, the moment coefficient C_M and thrust location x_m are referenced to the nozzle coordinate system whose origin is the center of the throat.

To obtain dimensional values for thrust F and moment M from the nondimensional coefficients, the following relationships are used:

$$F = A_t\, P_t\, C_F \tag{18}$$

$$M = A_t P_t y_t C_M \tag{19}$$

To compare theoretical results with experimental results, the following nondimensionalized relationships are applied:

$$\eta_X = C_{F,X_{\text{exp}}}/C_{F,X_{\text{th}}} \tag{20}$$

$$\eta_Y = C_{F,X_{\text{exp}}}/C_{F,Y_{\text{th}}} \tag{21}$$

$$\eta_\theta = \theta_{T_{\text{exp}}}/\theta_{T_{\text{th}}} \tag{22}$$

where η_X, η_Y, and η_θ are the efficiencies for axial thrust, side thrust, and thrust angle, respectively. Also, note the subscripts th and exp denote theoretical and experimental results, respectively.

Consideration must be given to the applicability of the result generated by the performance model. The value of $C_{F,X}$, $C_{F,Y}$, C_M, x_m, and θ_T are dependent on the following factors:

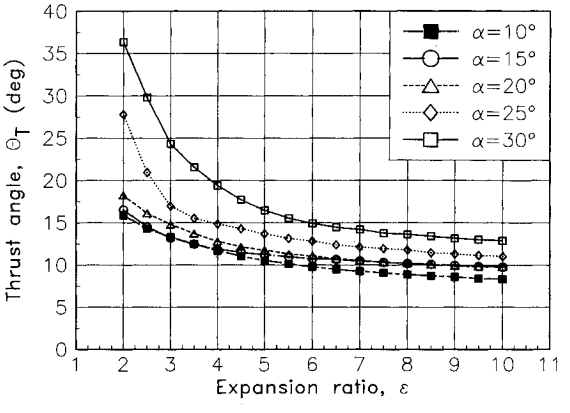

Fig. 4 Thrust angle as a function of expansion ratio for $P_a/P_t = 0$.

1) specific heat ratio γ; 2) nozzle geometry, ρ_{tu}/y_t, ρ_{td}/y_t, α, ϵ, β; and 3) operating condition P_a/P_t.

For a given nozzle geometry, the vacuum performance is applicable for all propellants with the same specific heat ratio and all operating conditions (P_a/P_t ratios) for which the flowfield analysis is valid.[1,3] By applying the relationships in Eqs. (9–17), the vacuum-performance results can be used to determine the actual nozzle performance at a given value of P_a/P_t. It should be noted that the relationships presented in Eqs. (14–17) are valid as long as the flowfield in the scarfed extension is not separated. As a practical matter, the methodology would be limited to cases where the pressure throughout the scarfed nozzle extension is greater than ambient to insure that the pressure force on the extension acts radially outward at all points. The limitation is not restrictive, as the side-force contribution of wall pressure must exceed that of the atmospheric pressure to achieve a side force that acts radially toward the missile axis. For a given nozzle geometry, this assumption effectively establishes a lower limit on the nozzle stagnation pressure for the practical utility of the concept.

Theoretical Study

To determine the influence of scarfed nozzle geometry and motor operating conditions on thrust-vector magnitude and orientation, an extensive parametric study was conducted utilizing the analysis model. The model was exercised for a wide range of variables that encompassed common design practices for tactical missile applications while preserving the assumptions of the model. The throat geometric specification ($\rho_{tu}/y_t = 1.0$, $\rho_{td}/y_t = 0.5$) and the specific heat ratio ($\gamma = 1.2$) were also selected as typical values for tactical solid propellant rocket motors. Two separate studies were performed—one considering the influence of design variables for the conical (basic) nozzle and the other considering scarfed extension design variables.

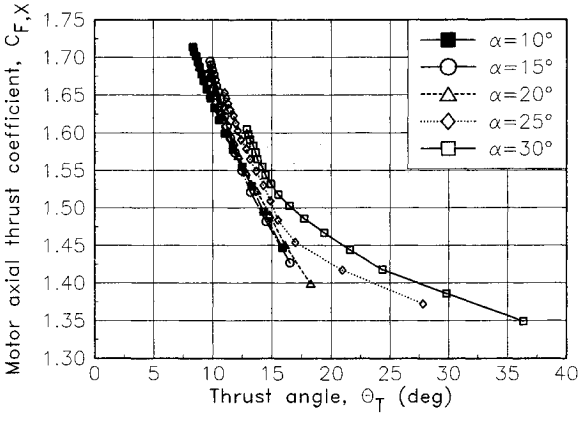

Fig. 5 Motor axial thrust coefficient as a function of thrust angle for $P_a/P_t = 0$.

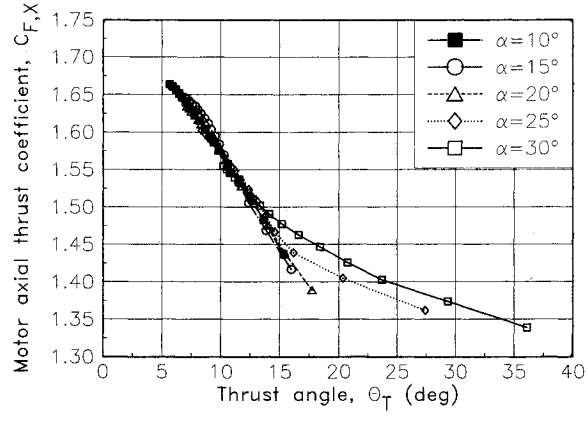

Fig. 6 Motor axial thrust coefficient as a function of thrust angle for $P_a/P_t = 0.005$.

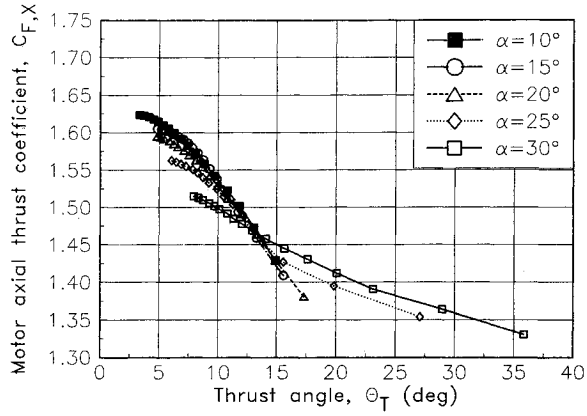

Fig. 7 Motor axial thrust coefficient as a function of thrust angle for $P_a/P_t = 0.009$.

Conical Nozzle Variables

For the primary study, a single scarf angle of 30 deg was selected in order to provide the longest possible scarfed extension length (maximizing side force) while not violating the criteria for maintaining axisymmetric flow throughout the nozzle.[4] Consequently, the conical nozzle independent variables in this study are α, ϵ, and P_a/P_t. The following set of independent variables were selected as typical for tactical rocket boosters: $\alpha = 10$, 15, 20, 25, 30 deg; $\epsilon = 2$, 3, 4, 5, 6, 7, 8, 9, and 10; and $P_a/P_t = 0.0$, 0.005, and 0.009. The upper limit of 0.009 for P_a/P_t assures a greater-than-atmospheric pressure throughout the scarfed extension for all combinations of α and ϵ considered.

Scarfed nozzle performance evaluations were conducted for all 135 combinations of α, ϵ, and P_a/P_t. The dependent performance factors of interest in this study were $C_{F,X}$, $C_{F,Y}$, and θ_T. It should be noted that the results for $P_a/P_t = 0.005$ and 0.009 were derived from the vacuum-performance result by applying Eqs. (9–17). The results of this parametric study are presented in Figs. 4–7.

Since the primary parameter of interest for this study was the amount of thrust-angle turning, the pertinent data are presented in relation to the thrust angle θ_T as defined by Eq. (17). A plot of thrust angle as a function of expansion ratio for vacuum conditions with nozzle half-angle as a parameter is shown in Fig. 4. In all cases, the nozzle half-angle is a significant control, particularly for the smaller expansion ratios. The driver for this large thrust turning is the strong shock induced by the cone-to-cylinder transition of the scarfed extension (see Fig. 2). The large relative angle between the cone and cylinder generates a high pressure behind the shock which then acts over the scarfed cylindrical extension to produce the large thrust angles shown in Fig. 4. In general, the statement can be made that thrust angle increases with half-angle and decreases with expansion ratio. This trend holds for all pressure ratios considered.

With such a significant capability to change the thrust angle, the question resolves itself into what nozzle design is best for a particular set of nozzle conditions. These conditions are usually dominated by missile system implications on the motor design, particularly for tactical missile applications. Plots of motor axial thrust coefficient, as a function thrust angle for P_a/P_t values of 0.00, 0.005, and 0.009, respectively, are shown in Figs. 5–7.

The interesting areas for study are the regions of smaller thrust angles (less than 15 deg) since large thrust angles can be achieved only for large nozzle half-angles and thrust angles less than 15 deg provide considerable design flexibility for actual use. The results in Fig. 5 for vacuum conditions show a measurable difference in motor axial thrust for a given thrust

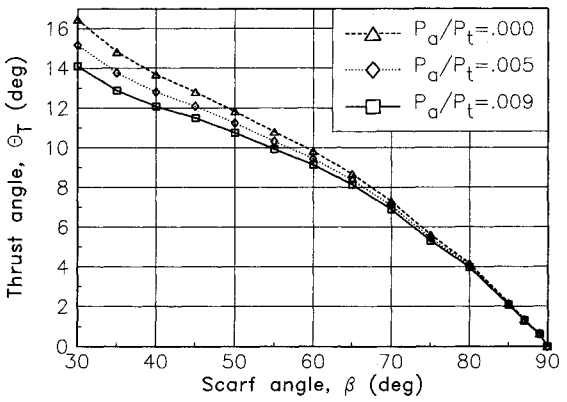

Fig. 8 Thrust angle as a function of scarf angle for $\alpha = 30$ deg, $\epsilon = 5$.

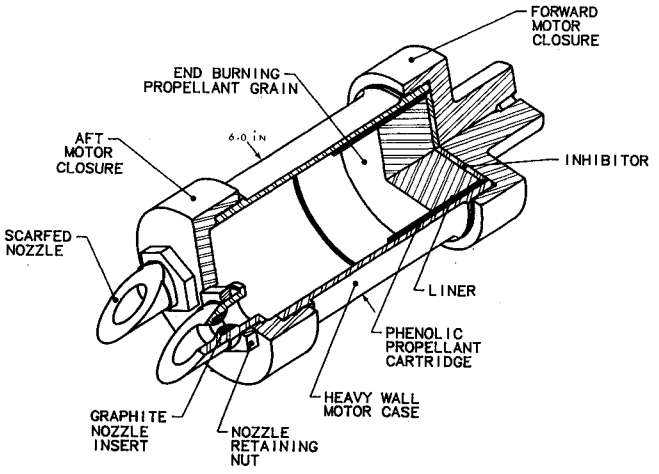

Fig. 9 Solid rocket motor cross section.

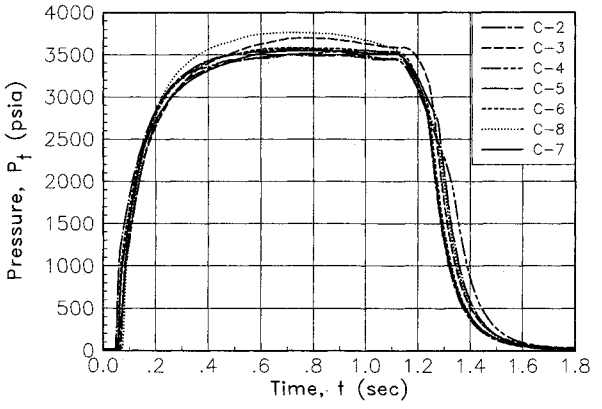

Fig. 10 Chamber pressure vs time.

angle with the higher nozzle half-angles providing higher axial thrust than nozzles with shallower half-angles. As the pressure ratio changes, so does the best choice of nozzle half-angles. For a pressure ratio of 0.005 (see Fig. 6), the motor axial thrust coefficient is virtually independent of nozzle half-angle for thrust less than 15 deg. As the pressure ratio becomes larger 0.009 (see Fig. 7), the shallower nozzles show a distinct advantage up to 15 deg thrust angle. From the results presented in Figs. 5–7, it is evident that the optimum half-angle for a given thrust angle is dependent on motor operating conditions (P_a/P_t).

Scarfed Extension Variable

A second parametric study was conducted to illustrate the influence of scarf angle (scarfed extension length) on thrust angle. The thrust angles determined in the first study represent a maximum. By increasing the scarf angle for a given nozzle beyond 30 deg, any thrust angle below that maximum can be achieved. Using a nozzle geometry of $\alpha = 30$ deg, $\epsilon = 5$, performance analyses were conducted for scarf angles between 30 and 90 deg at P_a/P_t values of 0.000, 0.005, and 0.009. The results are presented in Fig. 8. These results clearly demonstrate the ability to achieve a continuum of thrust angles from zero to the maximum by varying the scarf angle. This thrust-angle control allows the designer to select the basic nozzle design that represents the best compromise between axial performance and maximum available thrust angle. After the acquisition of experimental performance data and rocket design refinement, the scarf angle of the nozzle can be varied to fine tune the thrust angle without affecting the motor axial performance.

Table 1 Nozzle geometries

Motor	α, deg	ϵ
C-2	10	4.97
C-3	30	4.97
C-4	10	9.99
C-5	30	9.83
C-6	10	19.79
C-8	10	19.98
C-7	30	20.02

Model Validation

The theoretical model provided insight into the design flexibility available using the scarfed nozzle extension for control of the thrust angle. To validate the model, an experimental evaluation program was conducted utilizing existing hardware and test capabilities.

Test Hardware

Presented in Fig. 9 is a cutaway view of the heavywall solid rocket motor utilized in the experimental program. The salient features are an end-burning propellant grain to provide a flat pressure-time history and dual scarfed nozzles oriented to develop the maximum side force. The rocket motor was designed to operate at a constant 3600 psia chamber pressure to insure that the pressure levels were greater than ambient throughout the scarfed extension for all nozzles that were evaluated. Graphite nozzle-throat inserts were utilized to provide some degree of nozzle-throat erosion control to reduce experimental variability. The rocket motor was mounted horizontally in a test fixture and axial thrust, side thrust, and chamber pressure data were acquired and recorded for each firing.

Seven tests were performed to investigate the effect of nozzle half-angle and expansion ratio on thrust angle. Nozzle half-angles of 10 and 30 deg and expansion ratios of 5, 10, and 20 were tested and evaluated. Although outside of the range of interest, motors with expansion ratios of 20 were included in the experimental investigation due to the availability of existing nozzle hardware. The half-angle and expansion ratio for each motor test is shown on Table 1. For each motor firing, a theoretical performance analysis was conducted using average nozzle-throat geometries, a nominal stagnation pressure of 3600 psia, and a specific heat ratio determined by thermochemical analysis. Equations (9–17) were utilized to generate theoretical performance histories.

Figure 10 shows the pressure-time histories for the motor firings and clearly demonstrates the reproducible nature of the gas source provided by the solid-propellant motor. Although the pressure-time histories are very reproducible, there was some variation in the nozzle-throat erosion. In order to facilitate data reduction, the nozzle erosion was averaged for each test and the average nozzle dimension was used for the theoretical analysis. This should be manifested in the experimental thrust being higher than predicted toward the end of burning. Although this should not adversely affect the data trends, it

probably accounts for some of the progressivity apparent on the efficiency curves.

Data Analyses

Pressure, axial force, and side-force data were collected for the seven motors as configured in Table 1. For the purpose of model validation, the data were reduced to efficiencies as defined by Eq. (20–22). These efficiencies normalize the experimental results to the predicted results of the theoretical study. The experimental efficiency-time histories for axial thrust, side thrust, and thrust angle, respectively, are presented in Figs. 11–13. The theoretical predictions contain no ballistic efficiencies or nongeometric factors; therefore, the absolute values are not as important as the trends.

The bulk of the axial thrust-efficiency data presented in Fig. 11 shows a slight trend down during the first half of the burn and then a sharp upturn. This behavior is consistent with the existence of nozzle-throat erosion coupled with the use of an average throat radius for data-reduction simplicity. Although the variations between tests are but a few percentage points, it is noteworthy that tests C-2, C-6, and C-8 are all somewhat lower than the other tests and therefore further from the norm.

The abnormal behavior for axial thrust, the best understood parameter, makes the C-2, C-6, and C-8 experimental data highly suspect. The discrepancy between these three motor tests and the others is also apparent for the side force (Fig. 12) and in the thrust-angle efficiency (Fig. 13). The data from these suspect motors are shown there for completeness but are not considered appropriate for model validation. The remainder of the data do support very strongly the strength and validity of the model.

The experimental data from motors C-3, C-4, C-5, and C-7, which encompass nozzle half-angles of 10 and 30 deg and

Table 2 Summary of experimental results

Time intervals, s	Motor number	Measured thrust turning		
		θ_T, deg	η_θ	Ranking
0.2–0.3	C-3	13.2	0.957	1
	C-5	10.6	1.012	2
	C-2	10.1	1.100	3
	C-7	6.2	1.027	4
	C-4	5.3	0.967	5
	C-8	3.0	1.710	6
	C-6	2.4	1.388	7
0.3–0.4	C-3	13.2	0.948	1
	C-5	10.9	1.019	2
	C-2	10.3	1.114	3
	C-7	6.7	1.020	4
	C-4	5.5	0.966	5
	C-8	3.3	1.461	6
	C-6	2.7	1.234	7
0.6–0.7	C-3	13.4	0.957	1
	C-5	11.0	1.016	3
	C-2	11.8	1.260	2
	C-7	7.1	1.009	4
	C-4	5.6	0.960	5
	C-8	3.8	1.438	6
	C-6	3.2	1.261	7
0.7–0.8	C-3	13.6	0.972	1
	C-5	11.1	1.026	3
	C-2	12.2	1.301	2
	C-7	7.1	1.012	4
	C-4	5.7	0.973	5
	C-8	3.9	1.477	6
	C-6	3.3	1.301	7

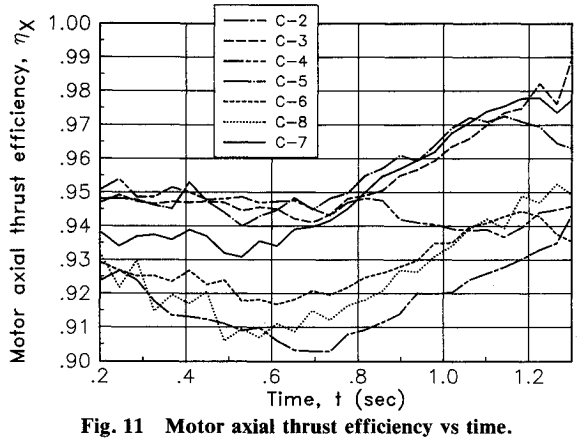

Fig. 11 Motor axial thrust efficiency vs time.

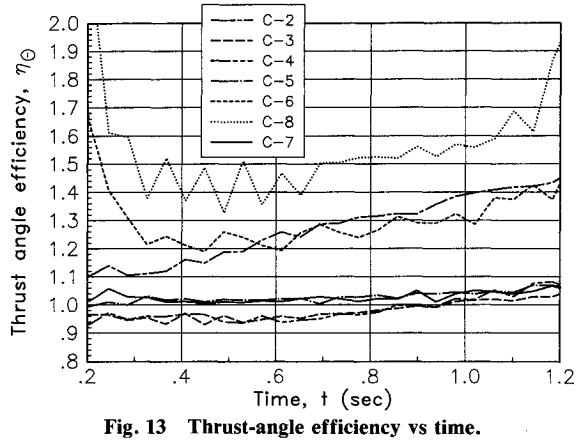

Fig. 13 Thrust-angle efficiency vs time.

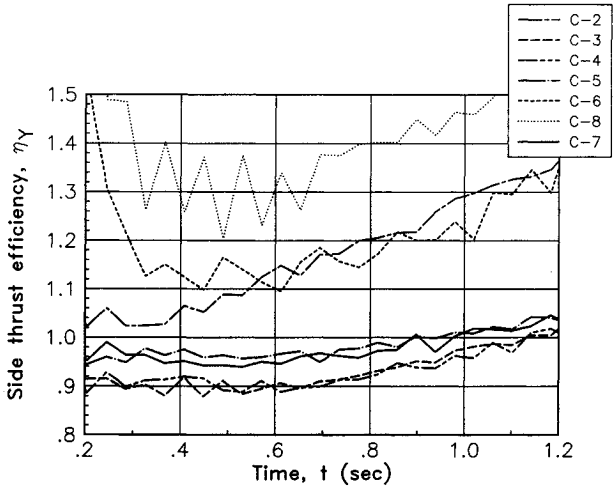

Fig. 12 Side thrust efficiency vs time.

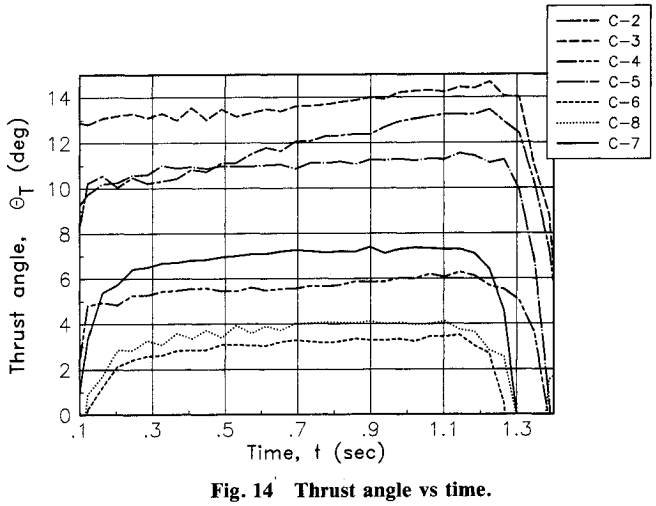

Fig. 14 Thrust angle vs time.

expansion ratios for 5–20, provide solid evidence for model validation. For these motors, the side-thrust efficiency (Fig. 12) and the thrust-angle efficiency (Fig. 13) are fairly constant with time and close to unity. The measured thrust angles of all tests are shown on Fig. 14. Disregarding motors C-2, C-6, and C-8, thrust angles from 5–14 deg have been demonstrated.

Table 2 is a summary of the experimental results taken at various time snapshots during each motor firing. The results are listed in descending order of predicted thrust turning. Presented in Table 2 are the measured values for the thrust turning angle, thrust-angle efficiency, and the relative ranking of the thrust turning based on experimental data. During the first half of the motor operation, the experimental performance is rank ordered as predicted. During the later part of the motor operation, motor 2 and motor 5 exchange ranking as motor 2, which is suspect, increases its deviation from predicted.

The results of the experimental program clearly demonstrate the ability of the model to predict the relative influence of expansion ratio and half-angle on thrust angle. Excluding the data from the suspect motors, the agreement between the theoretical and experimental results provides quantitative support for the model. The authors feel that quantitative differences evidenced by the suspect motors were a result of inadequancies in the test fixtures, not deficiencies in the model.

Limitations of the Concept

In order for the missile designer to fully exploit the use of scarfed nozzles for thrust-vector adjustment, the limitations of the concept must be understood. The primary applications for which this concept was formulated were tactical strap-on boosters that were assumed to be characterized by severely constrained diameters, high operating pressures, neutral (constant) chamber pressures, and constant operating altitudes (usually near the ground). These characteristic features impact the nozzle design by specifying, low-expansion ratios and near-zero and constant P_a/P_t values. Consequently, the scope of the theoretical study was limited to expansion ratios below 10 and P_a/P_t below 0.009 (P_a/P_t values were assumed to be constant for a given point design). Although the tactical booster provides the most attractive application for the concept, other applications can be considered. The analysis tools utilized in the present investigation can be employed to expand the theoretical results to include a wider range of nozzle designs and operational considerations. However, in the cause of any further design studies, it must be recalled that the underlying principal of the concept is the generation of a side force due to the pressure distribution in the scarfed extension. Consequently, the utility of the concept is diminished for systems that require higher expansion ratios and/or lower chamber pressures (higher P_a/P_t ratios) since a reduced pressure in the scarfed extension correspondingly reduces the thrust-vector adjustment capability. In addition, systems that experience large changes in altitude or large variations in chamber pressure due to throttling (large P_a/P_t variations) must be designed to tolerate corresponding changes in the thrust vector (as illustrated in Fig. 8).

Conclusions

A model was developed to analyze the performance of scarfed nozzles configured to control the motor thrust vector. This model was exercised for a wide range of nozzle geometries and motor pressure ratios. The results of the theoretical study indicate that a continuum of thrust angles up to 35 deg is available. Experimental tests for thrust angles up to 14 deg demonstrated the validity of the model. For many tactical rocket motor applications, the basic nozzle design is constrained by overall geometry, cost, and motor design requirements. The results of this investigation demonstrate that scarfed nozzles offer the propulsion system designer a low-cost, high-performance means of thrust-vector adjustment.

Acknowledgment

The authors wish to express their appreciation to the personnel of the Propulsion Directorate of the U. S. Army Missile Command, who provided invaluable support on this program in terms of hardware fabrication and assembly, propellant development and casting, and data acquisition and reduction.

References

[1]Lilley, J. S., and Hoffman, J. D., "Performance Analysis of Scarfed Nozzles," *Journal of Spacecraft and Rockets*, Vol. 23, Jan.–Feb. 1986, pp. 53–62.

[2]Hoffman, J. D., "A Computer Program for the Performance Analysis of Scarfed Nozzles," U. S. Army Missile Command, RK-CR-84-3, May 1984.

[3]Lilley, J. S., "Experimental Validation of a Performance Model for Scarfed Nozzles," *Journal of Spacecraft and Rockets*, Vol. 24, Nov.–Dec. 1987, pp. 474–480.

[4]Lilley, J. S., "The Analysis and Design of Scarfed Nozzles for Tactical Applications," U. S. Army Missile Command, RD-PR-86-2, Oct. 1986.